Multi-objective Day-ahead Polarity Switching Optimization for Voltage Unbalance in Bipolar DC Distribution Networks

Zhongchi Huang, Qianggang Wang, *Member*, *IEEE*, Yuan Chi, *Member*, *IEEE*, Jianquan Liao, *Member*, *IEEE*, Yu Zhang, and Niancheng Zhou, *Member*, *IEEE*

***Abstract*—Bipolar direct current (DC) distribution networks can effectively improve the connection flexibility for renewable generations and loads. In practice, concerns regarding the potential voltage unbalance issue of the distribution networks and the frequency of switching still remain. This paper proposes a day-ahead polarity switching strategy to reduce voltage unbalance by optimally switching the polarity of renewable generations and loads while minimizing the switching times simultaneously in the range of a full day. First, a multi-objective optimization model is constructed to minimize the weighted sum of voltage unbalance factors and the sum of number of switching actions in the day based on the power flow model. Second, a two-step solution strategy is proposed to solve the optimization model. Finally, the proposed strategy is validated using 11-node and 34-node distribution networks as case studies, and a switching and stabilizing device is designed to enable unified switching of renewable generations and loads. Numerical results demonstrate that the proposed strategy can effectively reduce the switching times without affecting the improvement of voltage balance.**

***Index Terms*—Bipolar direct current (DC) distribution network, multi-objective optimization, renewable generation, voltage unbalance.**

NOMENCLATURE

A. Indices and Sets

i	Index of time intervals ($i=1,2,\ldots,T$)
j	Index of nodes ($j=1,2,\ldots,M$)
k	Index of uncertainty scenarios ($k=1,2,\ldots,K$)
q	Index of dots on Pareto front ($q=1,2,\ldots,Q$)
r	Index of number of iterations in Newton-Raphson algorithm ($r=1,2,\ldots,R$)
s	Index of unipolar nodes ($s=1,2,\ldots,S$)

B. Parameters

$\boldsymbol{C}_1$	Vector consisting of $\boldsymbol{V}_{br}^{\min}$, $\boldsymbol{V}_{pnb}^{\min}$, and 0 (elements corresponding to $\boldsymbol{I}_{br}$ and $\boldsymbol{VUF}$ are 0)
$\boldsymbol{C}_2$	Vector consisting of $\boldsymbol{I}_{br}^{\max}$, $\boldsymbol{V}_{br}^{\max}$, $\boldsymbol{V}_{pnb}^{\max}$, and $\boldsymbol{VUF}^{\max}$
$\boldsymbol{E}$	Identity matrix
$\boldsymbol{E}_0$	Column vector of which all elements are 0
$\boldsymbol{E}_1$	Column vector of which all elements are 1
$\boldsymbol{G}$	Conductance matrix of network
$\boldsymbol{I}_{br}^{\max}$	Vector consisting of the maximum allowed value of each element in $\boldsymbol{I}_{br}$
i_{ZIP}	Parameter of constant current model
$\boldsymbol{O}$	Null matrix (dimension matches that of the formula)
P_0	Base power value for the ZIP model
$\boldsymbol{P}_{uni}$	Power vector of unipolar source/load
p_{ZIP}	Parameter of constant power model
pr	Probability corresponding to uncertainty scenario
$\boldsymbol{V}_{br}^{\max}$	Vector consisting of the maximum allowed value of each element in $\boldsymbol{V}_{br}$
$\boldsymbol{V}_{br}^{\min}$	Vector consisting of the minimum allowed value of each element in $\boldsymbol{V}_{br}$
$\boldsymbol{V}_{pnb}^{\max}$	Vector consisting of the maximum allowed value of each element in $\boldsymbol{V}_{pnb}$
$\boldsymbol{V}_{pnb}^{\min}$	Vector consisting of the minimum allowed value of each element in $\boldsymbol{V}_{pnb}$
$\boldsymbol{VUF}^{\max}$	Vector consisting of the maximum allowed value of each element in $\boldsymbol{VUF}$
z_{ZIP}	Parameter of constant resistance model

C. Variables

$\boldsymbol{C}$	Vector consisting of $\boldsymbol{I}_{br}$, $\boldsymbol{V}_{br}$, $\boldsymbol{V}_{pnb}$, and $\boldsymbol{VUF}$
$\boldsymbol{F}$	Multi-objective function vector
f_1	Objective function 1
f_2	Objective function 2

Manuscript received: August 26, 2022; revised: October 22, 2022; accepted: October 29, 2022. Date of CrossCheck: October 29, 2022. Date of online publication: December 15, 2022.

This work was supported by Fundamental Research Funds for the Central Universities (No. 2022CDJXY-007).

Z. Huang, Q. Wang, Y. Chi (corresponding author), and N. Zhou are with the Chongqing University, Chongqing, China (e-mail: 20163629@cqu.edu.cn; qianggang1987@cqu.edu.cn; chiyuanee@cqu.edu.cn; cee_nczhou@cqu.edu.cn).

J. Liao is with Sichuan University, Chengdu, China (e-mail: jquanliao@scu.edu.cn).

Y. Zhang is with State Grid Chongqing Shibei Electric Power Supply Branch, Chongqing, China (e-mail: zhangyu_023@163.com).

DOI: 10.35833/MPCE.2022.000539

$f_1^{\max}$	The maximum value of objective function 1 on Pareto front
$f_1^{\min}$	The minimum value of objective function 1 on Pareto front
$f_2^{\max}$	The maximum value of objective function 2 on Pareto front
$f_2^{\min}$	The minimum value of objective function 2 on Pareto front
$\boldsymbol{I}_{br}$	Branch current vector (absolute value)
$\boldsymbol{I}_{fl}$	Current vector in which current flows from other nodes to each node (excluding the node to which the voltage balancer belongs)
$\boldsymbol{I}_{mis}$	Mismatch current vector
$\boldsymbol{I}_{pnb}$	Current vector of positive, negative, and bipolar sources/loads
$\boldsymbol{J}$	Jacobian matrix
NSA	Number of switching actions (NSA)
$\boldsymbol{P}_{pnb}$	Power vector of positive, negative, and bipolar sources/loads
P_{ZIP}	Power of ZIP model
$SNSA$	Sum of NSA
u	Satisfaction degree of evaluating each point on Pareto front
$\boldsymbol{V}_{br}$	Voltage vector of of branch to ground at each node (excluding the node to which the voltage balancer belongs)
$\boldsymbol{V}_{pnb}$	Voltage vector of positive, negative, and bipolar sources/loads
V_{ZIP}	Voltage of ZIP model
VUF	Voltage unbalance factor (VUF)
$\boldsymbol{VUF}$	Vector of VUFs
$WSNSA$	Weighted sum of NSA considering probabilities of scenarios
$WSVUF$	Weighted sum of VUFs considering probabilities of scenarios
$\boldsymbol{X}$	Switching vector in a single time interval
$\boldsymbol{X}^i$	Switching vector in time interval i
$\boldsymbol{X}_{exp}$	Dimensionally expanded switching vector in a single time interval
$\boldsymbol{X}_m$	Switching vector representing switching state of every node in every time interval
$x^{i,s}$	Switching state of unipolar node s in time interval i
$\boldsymbol{Y}$	Binary vector that controls whether each switching vector in time interval i should be inverted
y	Binary element in $\boldsymbol{Y}$

I. Introduction

DIRECT current (DC) distribution networks have experienced accelerated development in recent years. Alternating current (AC)-DC conversion not only increases the transmission capacity but also helps boost the penetration level of renewable generations [1]. DC distribution networks also improve the power supply efficiency for DC loads such as electric vehicles, as the loss caused by AC-DC conversion can be avoided [2]. With the advantages of the DC distribution network, a bipolar DC distribution network represents a highly reliable DC system because the faults that occur in one line do not propagate to the other two lines [3]. In addition, the network is highly flexible, where the renewable generations or loads can be connected to the network in bipolar or unipolar form to obtain different bus voltages [4].

For a bipolar DC network, the unipolar access of renewable generations or loads may cause voltage unbalance, which deteriorates the power quality and efficiency [5]. In terms of devices, two common approaches can be used to mitigate the voltage unbalance, namely source- and load-side approaches. A typical source-side approach involves configuring the voltage balancer at the exit of the AC/DC rectifier [6], using the self-balancing isolated DC-DC converter [7], configuring the power flow controller at the head of the line [8], and using a three-level DC converter to balance the voltage [9]. These approaches are effective in controlling the local voltage, but their effectiveness is weakened for other nodes far from the controlled ones. A typical load-side approach involves configuring the voltage compensator [10] and using DC electric springs for regulation [5]. These approaches consider the voltage balance of the overall network and local nodes as long as global configuration is achieved. However, large-scale deployment of electronic devices will lead to significant operating losses. From a system perspective, common approaches for reducing voltage unbalance include regulating the sending-end voltage [11], using a static switch for load transfer [12], and switching the polarity of the load [2], [13]. However, the optimality of results has not been discussed [11], [12], and the switching of renewable generations, which is also an effective option for voltage balancing, has not been considered [2], [13].

For renewable generations such as wind generations, curtailment will waste resources [14]. To increase the utilization rate of renewable generations, it is possible to suppress the voltage unbalance by switching the polarity of renewable generations while maintaining the maximum output. To the best of our knowledge, no study has considered both renewable generations and loads as objects that can be switched in polarity to suppress voltage unbalance in bipolar DC distribution networks. To achieve this, a novel switch that provides both renewable generations and loads flexibility in switching should be designed. Reference [2] uses power electronic devices to realize polarity switching for loads. Although circuit breaking using power electronic devices is fast, the on-state losses are relatively high, which reduces the efficiency of the network [15]. Alternatively, a mechanical circuit breaker with small contact resistance can effectively solve this problem [15]. Although the breaking time is relatively long when compared with that of a hybrid low-voltage DC (LVDC) circuit breaker (tens of milliseconds vs. only a few milliseconds) [16], [17], the conventional mechanical circuit breaker is still more practical considering its cost and technological maturity. Prior to complete disconnection, the renewable gen-

eration or load is connected to a network through an arc, which leads to an unstable voltage. Moreover, a successful disconnection is usually followed by closing, and failures of the closing may occur due to an aging mechanical structure and electrical failure of equipment. Therefore, it is critical to maintain the stable operation of the renewable generations or loads during the switching time.

For a mechanical circuit breaker, frequent switching actions accelerate the aging process and exacerbate mechanical wear [15]. In addition to reduced reliability, replacing the switch frequently is economically disadvantageous due to excessive switching actions. In the optimization problem that takes the weighted sum of the voltage unbalance factors (WSVUF) as an objective, more switching times are generally favored because they can suppress voltage unbalance. Therefore, it is necessary to strike a balance between the mitigation of voltage unbalance and cost-efficient operation of switches. Previous studies have either simplified the problem as a static one, ignoring the number of switching actions (NSA) [13], or optimized the total NSA throughout a day in terms of time sequences and day-ahead planning [2]. Some studies have incorporated the variable similar to NSA that represents switching times as a constraint, and have included it in the fitness function or weighted objective function [18], [19], even though bipolar DC distribution networks are not the focus of these studies. For these approaches, it is difficult to objectively determine an appropriate threshold for the NSA and clearly reflect the impact of its change on the optimization results.

Regarding the solution method, a genetic algorithm (GA) is among the prevalent algorithms to address multi-objective optimization problems and is widely adopted for engineering problems. However, a direct implementation of a GA suffers from problems related to convergence speed and optimality of results. In [20], exponential calculations are used to increase the mutation rate for adaptive in-depth optimization, making the convergence effect random. In [21], the estimation of distribution algorithm (EDA) is not aimed at specific problems, and the feasible solutions obtained by sampling and filtering are found to be of limited help in the convergence of the GA.

To address the limitations of previous studies on this topic, a day-ahead polarity switching strategy is proposed in this paper to obtain the optimal day-ahead switching plan. The technical contributions of this paper are summarized as follows.

1) A multi-objective switching optimization model is proposed to simultaneously alleviate the voltage unbalance and extend the service life of the mechanical switch. Instead of considering the sum of NSA (SNSA) as a constraint, it is optimized as one of the objectives based on time sequence within a day.

2) A two-step solution strategy is proposed to reduce the computational burden of the model and accelerate the convergence of the solution algorithm. First, the minimum value of one objective is obtained on the premise that the other objective is the minimum. Second, the two obtained results are used as two initial individuals in the initial population of the multi-objective optimization problem, and then the GA is used to solve the original problem.

3) A novel topology design of a switching and stabilizing device (SSD) is proposed, and the corresponding switching principle is established to switch the polarity with a mechanical switch. The proposed SSD can reduce on-state losses, maintain stability during the switching process, and enable unified switching of renewable generations and loads, which are favorable for a distribution network.

II. Mathematical Model Based on Dynamic Switching of Source/Load

A. Overview of Network

Figure 1 illustrates the basic structure of a bipolar DC distribution network.

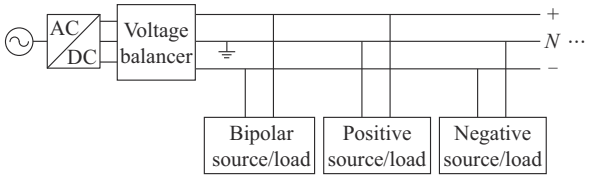

Fig. 1. Basic structure of bipolar DC distribution network.

Note that herein, "source/load" is used to represent an object that is either a renewable generation or load. The source/load can be connected to a network in a unipolar or bipolar manner. The unipolar source/load in the bipolar DC distribution network is connected to either the positive or negative pole. The values of unipolar voltage at the exit of the voltage balancer are considered equal.

B. Power Flow Model

Based on the method for iteratively solving the power flow model mentioned in [22], this paper establishes the relationship between the voltage of the source/load and the polarity switching vector.

The ZIP model (parallel connection of constant resistance, constant current and constant power loads) [22] is adopted to represent renewable generations and loads.

$$P_{ZIP}=P_0\left(z_{ZIP}V_{ZIP}^2+i_{ZIP}V_{ZIP}+p_{ZIP}\right) \tag{1}$$

When representing loads, all four parameters are positive. When representing renewable generations, because they are regarded as constant power sources, only P_0 and p_{ZIP} are retained (they are negative and positive, respectively), and the other parameters are 0.

It is assumed in this paper that either a renewable generation or load exists at each node. The switching vector $\boldsymbol{X}$ represents the polarity of each unipolar source/load in a time interval. When the element value is 1 or 0, the unipolar source/load at the corresponding node is switched to the positive or negative pole, respectively.

To facilitate the matrix calculation, $\boldsymbol{X}$ is rewritten as vector $\boldsymbol{X}_{exp}$, and its dimension is the sum of the number of unipolar and bipolar sources/loads. In $\boldsymbol{X}_{exp}$, the elements corresponding to the unipolar source/load still represent polarity in accordance with the aforementioned rule, and each ele-

ment corresponding to the bipolar source/load is 0. The relationship between the power of the sources/loads and $\boldsymbol{X}_{exp}$ is:

$$\boldsymbol{P}_{pnb}\left(\boldsymbol{X}_{exp}\right)=\begin{bmatrix}\boldsymbol{P}_p\left(\boldsymbol{X}_{exp}\right)\\ \boldsymbol{P}_n\left(\boldsymbol{X}_{exp}\right)\\ \boldsymbol{P}_b\end{bmatrix}=\begin{bmatrix}\mathrm{diag}\left(\boldsymbol{X}_{exp}\right)\\ \mathrm{diag}\left(\boldsymbol{E}_1-\boldsymbol{X}_{exp}\right)\\ \boldsymbol{O}\end{bmatrix}\boldsymbol{P}_{uni}+\begin{bmatrix}\boldsymbol{E}_0\\ \boldsymbol{E}_0\\ \boldsymbol{P}_b\end{bmatrix} \quad (2)$$

where the subscripts p, n, and b denote the positive, negative, and bipolar poles of the sources/loads, respectively.

To illustrate the power flow calculation, the case in which $\boldsymbol{X}_{exp}$ in (2) is fixed is considered first. In a general bipolar DC distribution network, the mismatch vector $\boldsymbol{I}_{mis}$ represents the difference between the current flowing into and out of each node [22].

$$\boldsymbol{I}_{mis}=\begin{bmatrix}\boldsymbol{I}_{mis,+}\\ \boldsymbol{I}_{mis,N}\\ \boldsymbol{I}_{mis,-}\end{bmatrix}=\boldsymbol{I}_{fl}-\begin{bmatrix}\boldsymbol{E}&\boldsymbol{O}&\boldsymbol{E}\\ -\boldsymbol{E}&\boldsymbol{E}&\boldsymbol{O}\\ \boldsymbol{O}&-\boldsymbol{E}&-\boldsymbol{E}\end{bmatrix}\boldsymbol{I}_{pnb} \quad (3)$$

where the subscripts +, N, and − denote the positive, neutral, and negative poles for the branches, respectively; and $\boldsymbol{I}_{pnb}=\left[\boldsymbol{I}_p^{\mathrm{T}},\boldsymbol{I}_n^{\mathrm{T}},\boldsymbol{I}_b^{\mathrm{T}}\right]^{\mathrm{T}}$.

$\boldsymbol{I}_{fl}$ can be expanded to $\boldsymbol{I}_{fl,vb}$, where the subscript vb indicates that the vector contains the node to which the voltage balancer belongs. $\boldsymbol{I}_{pnb}$ and $\boldsymbol{I}_{fl,vb}$ can be further expressed in terms of $\boldsymbol{V}_{br}=\left[\boldsymbol{V}_+^{\mathrm{T}},\boldsymbol{V}_N^{\mathrm{T}},\boldsymbol{V}_-^{\mathrm{T}}\right]^{\mathrm{T}}$ as:

$$\boldsymbol{I}_{pnb}=\begin{bmatrix}\boldsymbol{V}_{+,d}-\boldsymbol{V}_{N,d}&\boldsymbol{O}&\boldsymbol{O}\\ \boldsymbol{O}&\boldsymbol{V}_{N,d}-\boldsymbol{V}_{-,d}&\boldsymbol{O}\\ \boldsymbol{O}&\boldsymbol{O}&\boldsymbol{V}_{+,d}-\boldsymbol{V}_{-,d}\end{bmatrix}^{-1}\boldsymbol{P}_{pnb} \quad (4)$$

$$\boldsymbol{I}_{fl,vb}=\begin{bmatrix}\boldsymbol{I}_{fl,+,vb}\\ \boldsymbol{I}_{fl,N,vb}\\ \boldsymbol{I}_{fl,-,vb}\end{bmatrix}=-\begin{bmatrix}\boldsymbol{G}&\boldsymbol{O}&\boldsymbol{O}\\ \boldsymbol{O}&\boldsymbol{G}&\boldsymbol{O}\\ \boldsymbol{O}&\boldsymbol{O}&\boldsymbol{G}\end{bmatrix}\boldsymbol{V}_{br,vb} \quad (5)$$

where the subscript d denotes a diagonal matrix block.

By changing the dimension and substituting (1), (2), (4), and (5) into (3), we can obtain the mismatch vector as a function of $\boldsymbol{V}_{br}$, which is denoted as $\boldsymbol{I}_{mis}\left(\boldsymbol{V}_{br}\right)$.

The value of each element of $\boldsymbol{I}_{mis}$ should be zero when the voltage of each node is an accurate value. Thus, (6) can be obtained based on the Newton-Raphson algorithm [22].

$$\begin{cases}-\boldsymbol{I}_{mis}\left(\boldsymbol{V}_{br}^{(r)}\right)=\boldsymbol{J}\left(\boldsymbol{V}_{br}^{(r)}\right)\left(\boldsymbol{V}_{br}^{(r+1)}-\boldsymbol{V}_{br}^{(r)}\right)\\ \boldsymbol{J}=\begin{bmatrix}\dfrac{\partial\boldsymbol{I}_{mis,+}}{\partial\boldsymbol{V}_+}&\dfrac{\partial\boldsymbol{I}_{mis,+}}{\partial\boldsymbol{V}_N}&\dfrac{\partial\boldsymbol{I}_{mis,+}}{\partial\boldsymbol{V}_-}\\ \dfrac{\partial\boldsymbol{I}_{mis,N}}{\partial\boldsymbol{V}_+}&\dfrac{\partial\boldsymbol{I}_{mis,N}}{\partial\boldsymbol{V}_N}&\dfrac{\partial\boldsymbol{I}_{mis,N}}{\partial\boldsymbol{V}_-}\\ \dfrac{\partial\boldsymbol{I}_{mis,-}}{\partial\boldsymbol{V}_+}&\dfrac{\partial\boldsymbol{I}_{mis,-}}{\partial\boldsymbol{V}_N}&\dfrac{\partial\boldsymbol{I}_{mis,-}}{\partial\boldsymbol{V}_-}\end{bmatrix}\end{cases} \quad (6)$$

The iteration continues until the norm of $\boldsymbol{I}_{mis}$ becomes smaller than the positive value set in advance.

When $\boldsymbol{X}$ changes, the voltage of the network changes, and different voltage vectors can be obtained through the previous steps. The relationship between $\boldsymbol{V}_{br}$ and $\boldsymbol{X}$ is denoted as $\boldsymbol{V}_{br}(\boldsymbol{X})$. The relationship between the voltages of the sources/loads and $\boldsymbol{X}$ is expressed as:

$$\boldsymbol{V}_{pnb}(\boldsymbol{X})=\begin{bmatrix}\boldsymbol{E}&-\boldsymbol{E}&\boldsymbol{O}\\ \boldsymbol{O}&\boldsymbol{E}&-\boldsymbol{E}\\ \boldsymbol{E}&\boldsymbol{O}&-\boldsymbol{E}\end{bmatrix}\boldsymbol{V}_{br}(\boldsymbol{X}) \quad (7)$$

C. Optimization Model

1) Decision Variables

The decision variable in this paper is the switching state $x^{i,s}$ of unipolar node s in the time interval i. The switching vector $\boldsymbol{X}_m$ consists of the switching states of every unipolar node in every time interval.

2) Objective Functions

This paper divides a day into T time intervals. The parameters of the loads and renewable generations change in different time intervals and can be regarded as constant in a single time interval to facilitate the optimization calculation. In this paper, stochastic programming [23], [24] is used to address the uncertainty problem of renewable generations. The Monte Carlo method is used to obtain different scenarios, and the backward scenario reduction method is used to reduce the number of scenarios. The probability of each scenario is reflected in each objective function in the form of weights.

If the unipolar sources/loads in the bipolar distribution network are not properly distributed, the positive and negative voltages of the network will be unbalanced, which will increase the neutral current and network losses, and reduce network efficiency. Regarding the expression of voltage unbalance, the analogy from AC is to divide the absolute value of the difference between the positive and negative voltage values by the average of the two values [11]. This quantity is referred to as the voltage unbalance factor (VUF) in this paper. The WSVUF of all nodes in all time intervals during a day is the first objective of the proposed optimization model for representing the voltage unbalance of the network, which can be written as:

$$f_1\left(\boldsymbol{X}_m\right)=WSVUF\left(\boldsymbol{X}_m\right)=\sum_{k=1}^{K}\left(pr^k\cdot\sum_{i=1}^{T}\sum_{j=1}^{M}VUF^{i,j,k}\left(\boldsymbol{X}^i\right)\right)=$$
$$\sum_{k=1}^{K}\left[pr^k\cdot\sum_{i=1}^{T}\sum_{j=1}^{M}\frac{\left|V_p^{i,j,k}\left(\boldsymbol{X}^i\right)-V_n^{i,j,k}\left(\boldsymbol{X}^i\right)\right|}{0.5\left(V_p^{i,j,k}\left(\boldsymbol{X}^i\right)+V_n^{i,j,k}\left(\boldsymbol{X}^i\right)\right)}\right] \quad (8)$$

The service life of a mechanical switch is closely related to the NSA throughout its lifecycle. Reducing the NSA, which in turn alleviates mechanical wear, is beneficial to the service life and is ultimately cost-saving. The second objective, after simplification, is the SNSA within a day, which can be written as:

$$f_2\left(\boldsymbol{X}_m\right)=WSNSA\left(\boldsymbol{X}_m\right)=\left(pr^k\cdot\sum_{i=2}^{T}NSA^i\left(\boldsymbol{X}^i,\boldsymbol{X}^{i-1}\right)\right)=$$
$$\sum_{i=2}^{T}\sum_{s=1}^{S}\left|x^{i,s}-x^{i-1,s}\right|=SNSA\left(\boldsymbol{X}_m\right) \quad (9)$$

Since the weighted sum is equal to the sum when count-

ing switching actions, the latter is used instead of the former. The NSA from the initial distribution to the distribution in the first time interval is not counted in the SNSA.

Voltage unbalance and excessive switching actions have adverse effects on the operation and maintenance costs of DC distribution networks. To reduce these adverse effects, two objectives, i.e., WSVUF and SNSA, are incorporated into a multi-objective optimization model. The overall objective function is expressed as:

$$\min \boldsymbol{F}\left(\boldsymbol{X}_m\right)=\left[f_1\left(\boldsymbol{X}_m\right), f_2\left(\boldsymbol{X}_m\right)\right]^{\mathrm{T}} \tag{10}$$

3) Constraints

The constraints of the branch current, voltage of the branch to the ground, voltage of the source/load, and VUF are expressed as:

$$\begin{cases}\boldsymbol{I}_{br}\left(\boldsymbol{X}_m\right) \le \boldsymbol{I}_{br}^{\max} \\ \boldsymbol{V}_{br}^{\min} \le \boldsymbol{V}_{br}\left(\boldsymbol{X}_m\right) \le \boldsymbol{V}_{br}^{\max} \\ \boldsymbol{V}_{pnb}^{\min} \le \boldsymbol{V}_{pnb}\left(\boldsymbol{X}_m\right) \le \boldsymbol{V}_{pnb}^{\max} \\ \boldsymbol{VUF}\left(\boldsymbol{X}_m\right) \le \boldsymbol{VUF}^{\max}\end{cases} \tag{11}$$

These constraints ensure that the network can operate safely, and are rewritten as:

$$\boldsymbol{C}_1 \le \boldsymbol{C}\left(\boldsymbol{X}_m\right) \le \boldsymbol{C}_2 \tag{12}$$

III. Two-step Solution Strategy

The optimization model constructed in this paper is highly nonlinear and has two conflicting objectives that can hardly be solved. The GA has proven to be effective in solving multi-objective problems [25] and thus is adopted in this paper. To reduce the computational burden of the model and accelerate convergence, a two-step solution strategy is proposed based on the time-series correlation of renewable generations or loads and the iterative principle of the GA. This strategy makes full use of the solution results of sub-problems, thereby providing a method for generating the initial population that can assist in performing optimization calculations.

A. Step 1

The purpose of *Step 1* is to obtain two estimated switching plans as the initial individuals of the GA to improve optimality and reduce the computational burden in *Step 2*. The first estimated plan aims to determine the smallest SNSA when the WSVUF has the smallest value. The second estimated plan aims to find the smallest WSVUF when the SNSA is 0. Therefore, *Step 1* is divided into two parts to obtain the two estimated switching plans.

In the previous calculation of the first part, the sub-objective f_2 is ignored, and the single-objective optimization model is constructed independently for the network in each time interval.

The optimization model in time interval i is expressed as:

$$\min \sum_{k=1}^{K}\left(pr^k \cdot \sum_{j=1}^{M} VUF_{pre}^{i,j,k}\left(\boldsymbol{X}_{pre}^{i}\right)\right) \tag{13}$$

s.t.

$$\begin{cases}x_{pre}^{i,1}=1 \\ \boldsymbol{C}_{1,c} \le \boldsymbol{C}_c^i\left(\boldsymbol{X}_{pre}^{i}\right) \le \boldsymbol{C}_{2,c}\end{cases} \tag{14}$$

where the subscript *pre* denotes that the result obtained by solving (13) and (14) is that of the previous calculation of the first estimated plan; and the subscript c denotes that the vector dimension is reduced to a dimension suitable for a single time interval.

For a specific time interval and the network with only one node connected to the voltage balancer node, two inverted switching plans (i.e., for every element, 0 becomes 1 and 1 becomes 0) are obtained if the VUF has the same value. Considering that T time intervals exist, 2^T different estimated plans are possible. To ensure that the optimization result in the previous calculation is unique, this paper restricts the switching state of the first node with a unipolar source/load to 1. Since the polarity of the first unipolar node is unknown in practice, it is not constrained in the following models.

When solving (13) and (14), the solution result of the problem in the previous time interval is used as one of the initial individuals when solving the problem in the next time interval. This can be explained as follows. In practice, for the renewable generation or load of a particular node, the power value of the next time interval has a time-series correlation with that of the previous time interval. This time-series correlation derives from the change in user electricity consumption in two adjacent time intervals or the change in the output of renewable generations due to meteorological changes. Based on this correlation, the algorithm benefits by searching results using the previous result as one of the initial individuals rather than by randomly generating initial individuals.

Thus far, the optimal solution is obtained only in terms of the WSVUF, and the optimality of the SNSA in this solution is not considered. As previously discussed, the WSVUF will not change if any $\boldsymbol{X}^i$ is inverted; thus, the optimal SNSA can be obtained as long as optimizing whether the vector derived from solving (13) and (14) in every time interval is inverted. A binary vector $\boldsymbol{Y}$ with dimension T is proposed to control whether $\boldsymbol{X}_{pre}^{i}$ in each time interval is inverted. The optimization model can be expressed as:

$$\begin{aligned}\min SNSA_{first}\left(\boldsymbol{X}_{m,first}(\boldsymbol{Y})\right)=\sum_{i=2}^{T}\sum_{s=1}^{S}\Big|&\left(1-y^i\right)\left(1-x_{pre}^{i,s}\right)+y^i x_{pre}^{i,s}- \\ &\left(1-y^{i-1}\right)\left(1-x_{pre}^{i-1,s}\right)-y^{i-1}x_{pre}^{i-1,s}\Big|\end{aligned} \tag{15}$$

s.t.

$$\boldsymbol{C}_1 \le \boldsymbol{C}_{first}\left(\boldsymbol{X}_{m,first}(\boldsymbol{Y})\right) \le \boldsymbol{C}_2 \tag{16}$$

where the subscript *first* denotes that the result obtained by solving (15) and (16) is that of the first estimated plan, and (16) can be ignored if the security constraints are confirmed not to be violated after inverting.

According to the solution of the optimization model in (13), (14) (in every time interval) and that in (15), (16), the first estimated plan can be obtained.

The second part is to seek the minimum WSVUF when

the SNSA is 0.

$$\min WSVUF_{second}\left(\boldsymbol{X}_{m,second}\right)=\sum_{k=1}^{K}\left(pr^{k}\cdot\sum_{i=1}^{T}\sum_{j=1}^{M}VUF_{second}^{i,j,k}\left(\boldsymbol{X}_{second}\right)\right) \tag{17}$$

s.t.

$$\boldsymbol{C}_1\le\boldsymbol{C}_{second}\left(\boldsymbol{X}_{m,second}\right)\le\boldsymbol{C}_2 \tag{18}$$

where the subscript *second* indicates that the result obtained by solving (17) and (18) is that of the second estimated plan.

Because the SNSA is zero, $\boldsymbol{X}^i$ is the same for each time interval. Therefore, $\boldsymbol{X}^i$ is represented by $\boldsymbol{X}_{second}$ in (17), which is an *S*-dimensional vector.

B. Step 2

In *Step 2*, the proposed multi-objective optimization model is solved.

$$\min \boldsymbol{F}(\boldsymbol{X}_{m,mul})=\left[f_1\left(\boldsymbol{X}_{m,mul}\right),f_2\left(\boldsymbol{X}_{m,mul}\right)\right]^{\mathrm{T}} \tag{19}$$

s.t.

$$\boldsymbol{C}_1\le\boldsymbol{C}_{mul}\left(\boldsymbol{X}_{m,mul}\right)\le\boldsymbol{C}_2 \tag{20}$$

where the subscript *mul* indicates the results obtained by solving (19) and (20) are those derived from solving the multi-objective optimization model.

The two estimated plans obtained in *Step 1* are used as two initial individuals in the initial population of the GA, and the other individuals are randomly generated. After the Pareto front is obtained, the fuzzy membership method [26] is used to select the final optimization result, which represents a compromise. The method for obtaining the membership is given as:

$$u^q=\frac{\dfrac{f_1^{\max}-f_1^q}{f_1^{\max}-f_1^{\min}}+\dfrac{f_2^{\max}-f_2^q}{f_2^{\max}-f_2^{\min}}}{\displaystyle\sum_{q=1}^{Q}\left(\frac{f_1^{\max}-f_1^q}{f_1^{\max}-f_1^{\min}}+\frac{f_2^{\max}-f_2^q}{f_2^{\max}-f_2^{\min}}\right)} \tag{21}$$

where the two objective functions represented by each point on the Pareto front are f_1^q and f_2^q, respectively.

In (21), u^q is calculated. The switching plan corresponding to the highest value is selected as the final switching plan.

C. Computational Steps of Proposed Strategy

The computational steps of the proposed strategy are shown in Fig. 2.

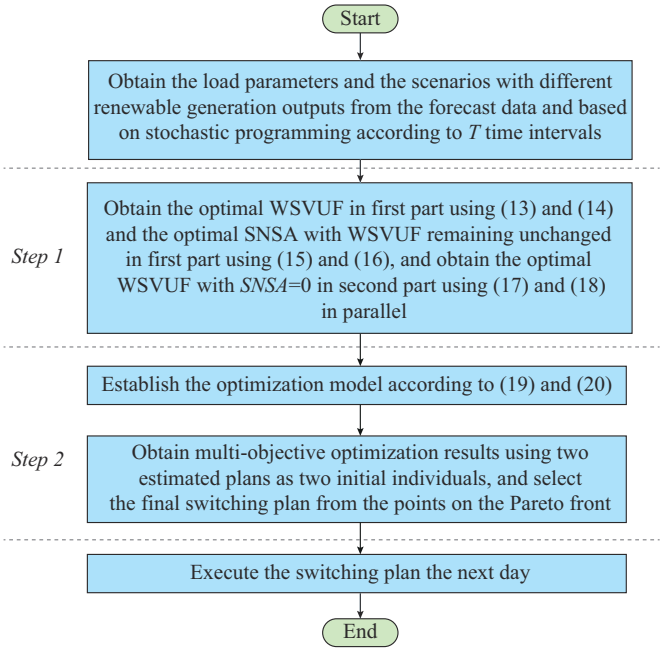

Fig. 2. Computational steps of proposed strategy.

IV. Case Study

A. Test System and Parameter Settings

In this paper, 11-node and 34-node distribution networks are used to validate the proposed strategy. In the strategy, a switching decision is made every 30 min, and 48 decisions are optimized. The constraint data can be found in Appendix A.

The 11-node distribution network contains 5 unipolar loads, 2 bipolar loads, and 3 unipolar renewable generations. The topology of the 11-node distribution network with the initial distribution of sources/loads is shown in Fig. 3.

To reflect electrical engineering practices, the load at node 7 and the renewable generation at node 8 are set to always maintain the same polarity. The pair is used to represent the scenario in which the electric energy generated by a renewable generation is first transmitted to the nearby load; if electric energy is in surplus, it will be transmitted to the distribution network, and if the electric energy is insufficient, it will be replenished from the distribution network. In this network, the sources/loads at nodes 2-5 and 7-10 are switchable; thus, the dimension of $\boldsymbol{X}^i$ in this network is 7, and each element corresponds to the state of the above node in order (where the 5th element represents the states of the load and renewable generation at nodes 7 and 8, respectively). The initial distribution shown in Fig. 3 can be represented by $[1,0,0,0,0,0,1]^{\mathrm{T}}$. The voltage at the exit of the voltage balancer is 375 V at the positive and negative poles.

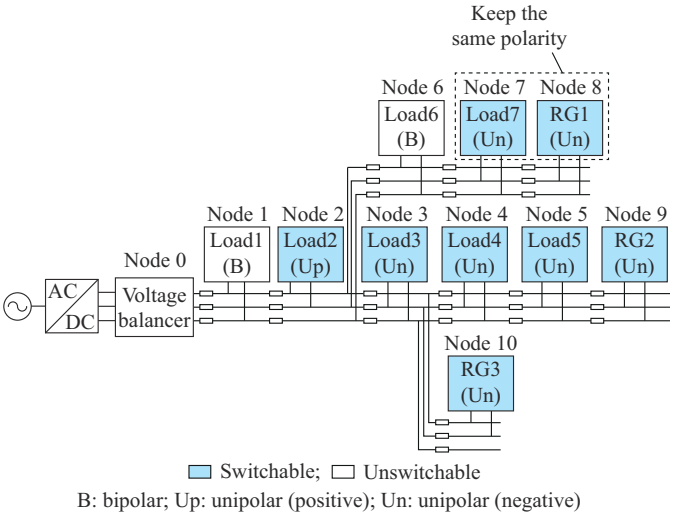

Fig. 3. Topology of 11-node distribution network with initial distribution of sources/loads.

The 34-node distribution network contains 14 unipolar loads, 9 bipolar loads, and 10 unipolar renewable generations. The topology of the 34-node distribution network with the initial distribution of sources/loads is shown in Fig. 4.

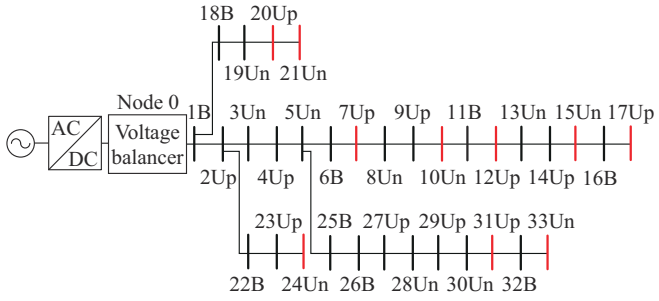

B: bipolar; Up: unipolar (positive); Un: unipolar (negative)

Fig. 4. Topology of 34-node distribution network with initial distribution of sources/loads.

In Fig. 4, the black and red nodes indicate that the node is connected to a load and renewable generation, respectively. In this network, the sources/loads at the unipolar nodes are switchable. The polarity states of the different switchable sources/loads are independent of each other. The voltage at the exit of the voltage balancer is 750 V at the positive and negative poles.

In the case studies, the renewable generations are considered as wind power generations. Considering the uncertainty of wind power generations, 1000 initial scenarios are first generated based on the Monte Carlo method. Then, through the backward scenario reduction method, the number of scenarios is reduced to five, and the corresponding probability is obtained, as shown in Fig. 5.

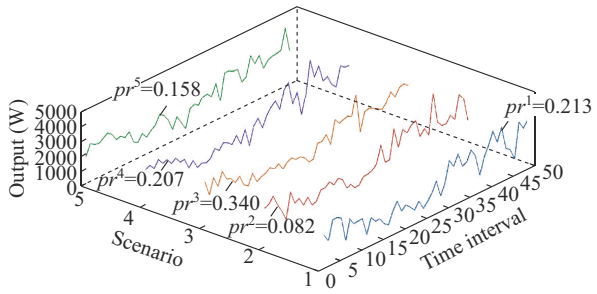

Fig. 5. Wind power generation scenarios and corresponding probabilities.

This paper assumes that the output values of the wind power generations at different nodes are the same in each scenario. The optimization problems are solved using the GA. The crossover and mutation rates are set to be 0.8 and 0.05, respectively. A two-point crossover strategy has been adopted. The tolerances for the function are 10^{-6} and 10^{-4} when solving single- and multi-objective optimization problems, respectively. The population size and iteration limit are presented in Appendix A.

B. Design and Verification of SSD

The SSD is designed to switch the unipolar source/load and ensure that it remains stable during the switching process. Compared with power electronic switching devices [2], SSDs have the advantages of lower on-state losses and of providing an effective means for obtaining and releasing electric energy during the switching process.

The SSD comprises four switching units (SUs) and a backup capacitor (Cb). Each SU consists of a mechanical circuit breaker, a disconnector and an RL parallel unit in series. Figure 6 shows the topology of the SSD and its three states when switching a unipolar load from the positive pole to the negative pole. The lines with different colors represent the current paths (red, blue, and green lines indicate the current path before, during, and after switching, respectively). For convenience in showing different states, two disconnectors and two breaking parts of the circuit breaker in each SU are shown in the figure.

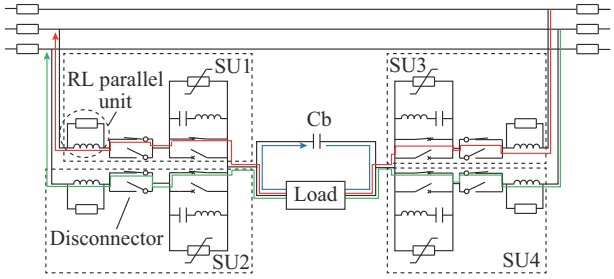

Fig. 6. Topology of SSD and its three states when switching unipolar load from positive pole to negative pole.

The functions of the mechanical DC circuit breaker and the disconnector in series involve disconnecting the DC current by self-excited oscillation [27] and closing. RL parallel units are used to suppress the impulse current that may occur at the moment of closing.

With the switching action in Fig. 6 used as an example, the switching principle of SSD for the load is presented in Fig. 7.

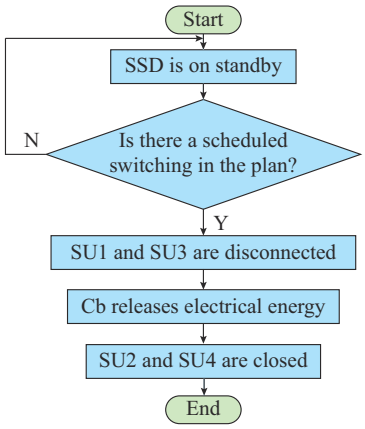

Fig. 7. Switching principle of SSD for load.

When switching the positive load, the two SUs connected to the positive pole are disconnected. The load is then energized for a short time by the capacitor until the two SUs connected to the negative pole are closed.

To verify the function and effect of the SSD, a simulation has been built in MATLAB/Simulink. The computer setup is

an Intel i5-1038NG7 CPU (16 GB RAM). Note that DC circuit breakers that extinguish arcs through self-oscillation have been manufactured for many years. The effects of inductance and capacitance selection on self-oscillation are described in [28]. In our simulation, an ideal switch is used in each SU to replace the disconnector and circuit breaker. This substitution may have caused the simulated waveform to differ slightly from the actual waveform, but the deviation has little impact on verifying the effects of the design on the polarity switching and voltage maintenance. The capacitance of each Cb is set to be 0.1 F (the internal resistance is 0.02 Ω). The series equivalent resistance of each ideal switch is set to be 0.0005 Ω. The values of the resistance and inductance of the RL parallel unit are 0.5 Ω and 0.01 H, respectively [29]. The internal resistance of the inductive component is 0.01 Ω. The voltage balancer is considered as constant voltage sources, and each internal resistance is set to be the same to the resistance of the branch from the voltage balancer node to the first node

In the simulation, the connection that relies on the arc is ignored, and the source/load is regarded as completely disconnected from the network during the switching process. The sum of the disconnection time, closing time, etc., is considered as the switching time, which is set to be 70 ms in the simulation. Because the time gap between the two switching actions set in this study is 30 min, and the time of the switching process is measured in tens of milliseconds, for the sake of observation, the time gap is shortened to be 5 s in the simulation. This has also been done considering that the network is basically stable after switching.

The power data for time intervals 9-11 of the 11-node distribution network in Scenario 1 are used for the simulation. Assuming that the switching states could be represented by $[1, 0, 1, 0, 1, 0, 1]^{\mathrm{T}}$ in time interval 9, we observe the switching actions in the following two time intervals. Nodes 3 and 10 are used as examples of switching a load (as shown in Fig. 8) and switching a renewable generation (as shown in Fig. 9), respectively. The red, blue, and green lines represent the current of the positive circuit breaker, the current of the negative circuit breaker, and the voltage of the unipolar source/load, respectively. The step size is 10^{-4} s, and the time values required to obtain the simulation results are 84.5 s and 84.8 s, respectively.

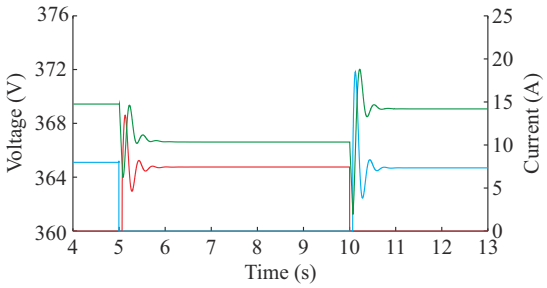

Fig. 8. Simulation results of switching load at node 3.

In Fig. 8, from the current changes, it can be observed that the SSD realizes the function of switching a load between the positive and negative poles. Similarly, from the voltage changes, it can be observed that Cb achieves a stabilizing effect on the load during the switching process, i. e., the power supply to the load is uninterrupted.

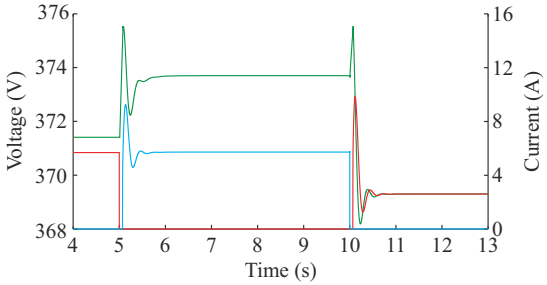

Fig. 9. Simulation results of switching renewable generation at node 10.

Figure 9 shows a similar function and effect of the SSD on renewable generations. The SSD realizes the function of switching a renewable generation between positive and negative poles, and the role of the renewable generation as an energy supplier is uninterrupted during the process. We can observe that the SSD enables unified switching of renewable generations and loads.

C. Proposed Strategy for an 11-node Distribution Network (Case 1)

Case 1 is used to verify the effectiveness of the proposed strategy on an 11-node distribution network. Because the time interval between the two switching actions is much longer than the switching time, the role of the SSD is ignored in the optimization calculation, and the switching is considered to be completed instantaneously. The internal resistance of each voltage source is also ignored.

In *Step 1*, two estimated switching plans have been derived, as shown in Fig. 10. The shadowed and white blocks indicate that the source/load is switched to the positive and negative poles, respectively. If the first estimated plan is adopted, the WSVUF and SNSA will be 1.161 and 84, respectively; if the second estimated plan is adopted, the WSVUF and SNSA will be 1.372 and 0, respectively.

In *Step 2*, several alternative switching plans have been derived. The Pareto front for Case 1 is shown in Fig. 11.

In the alternatives, the WSVUF can be reduced by as much as 87.87% compared with that of the initial distribution of sources/loads. The satisfactory degree of each switching plan is calculated using the fuzzy membership method, and the switching plan corresponding to the highest satisfactory degree is selected as the final result. The selected plan is marked by a red dot in Fig. 11. If the final switching plan is adopted, the WSVUF will be 1.212, which is reduced by 87.34%, and the SNSA will be 42. The final switching plan for Case 1 is shown in Fig. 12.

A comparison between the VUF of each node in the initial configuration state and that of the final switching plan in Case 1 is shown in Fig. 13 (the parameter data in Scenario 1 are used). The black line represents the change in VUF when the initial distribution does not change during the day, and the red line represents the change in VUF when the final switching plan obtained for Case 1 is adopted.

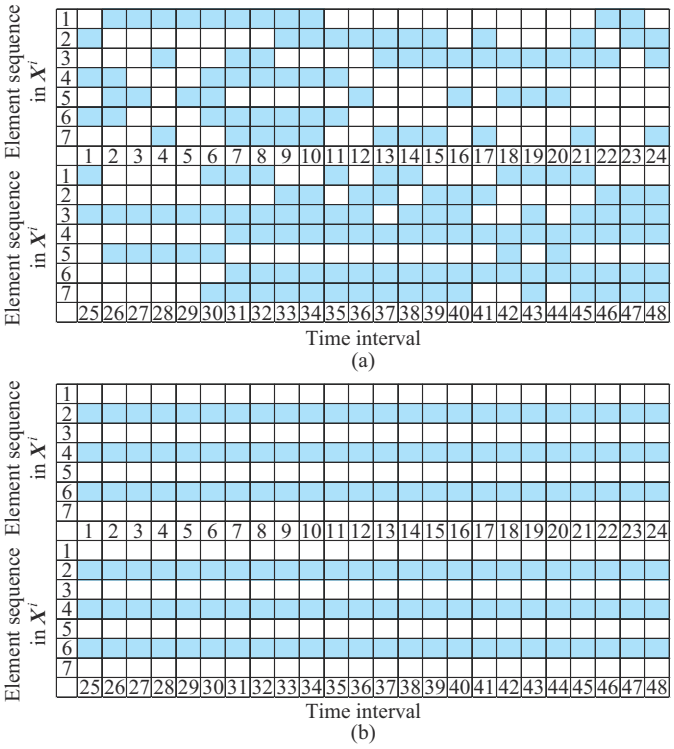

Fig. 10. Two estimated switching plans. (a) The first estimated switching plan. (b) The second estimated switching plan.

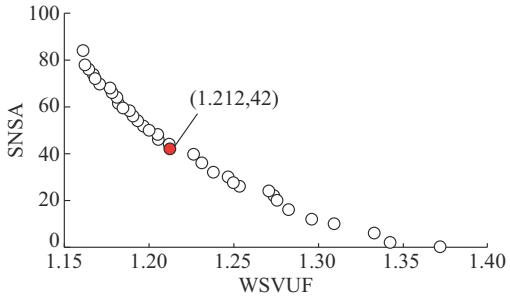

Fig. 11. Pareto front for Case 1.

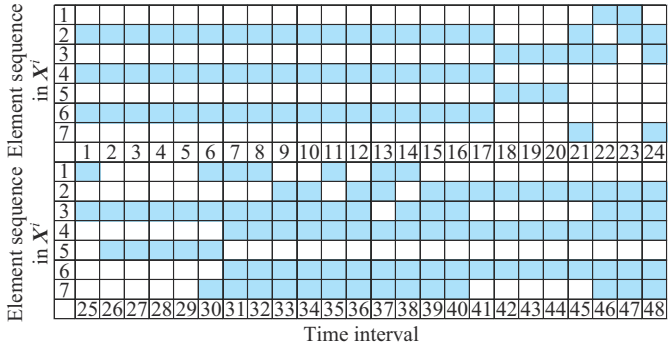

Fig. 12. Final switching plan for Case 1.

As Fig. 13 shows, the VUF in the bipolar DC distribution network is significantly reduced after the final switching plan is adopted. The VUF of each node is suppressed to be below the limit (3%). Although node 8 in the early and final time intervals experiences higher VUFs, the sum of VUFs of the overall network in Scenario 1 is reduced by 87.18% as compared with that of the initial distribution of sources/loads.

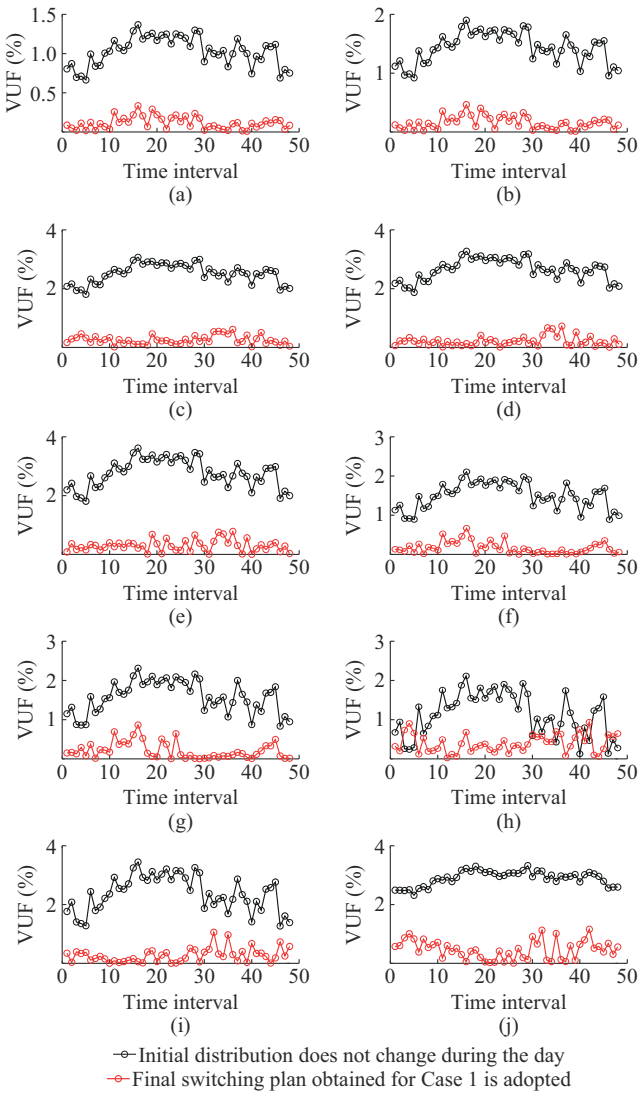

Fig. 13. VUFs of different nodes for Case 1 (Scenario 1). (a) Node 1. (b) Node 2. (c) Node 3. (d) Node 4. (e) Node 5. (f) Node 6. (g) Node 7. (h) Node 8. (i) Node 9. (j) Node 10.

D. Proposed Strategy for a 34-node Distribution Network (Case 2)

Case 2 is used to verify the effectiveness and scalability of the proposed strategy in this paper on a 34-node distribution network.

Based on the optimization model and solution strategy proposed in this paper, Fig. 14 shows the obtained Pareto front and results of the selected plan (red dot).

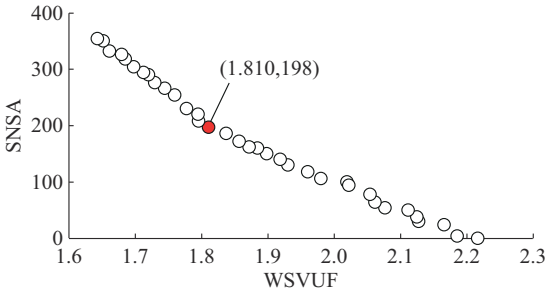

Fig. 14. Pareto front for Case 2.

If the plan is adopted, the WSVUF and SNSA will be 1.810 and 198, respectively. Compared with the initial distribution, the WSVUF is reduced by 70.11%. We can see that the proposed strategy also has good effect in a network with a larger number of nodes.

E. Cases for Comparison

To demonstrate the advantages of the proposed strategy, four additional methods (Cases 3-6) are used for comparison and are described in Table I.

TABLE I
DESCRIPTION OF CASES FOR COMPARISON

Case	Method
3	Method ignoring SNSA
4	Method without the two-step solution strategy
5	Method using SNSA as constraint
6	Neutral to line drop compensation (NLDC) method

In each case, the method is tested on the 11-node distribution network, and the role of the SSD is ignored. The internal resistance of each voltage source is also ignored.

1) Cases 3-5

Case 3 is used to illustrate the superiority of the proposed strategy by comparing the solution results with the proposed strategy and those that ignores the SNSA.

Case 4 is used to compare the differences between the solution results without and with the two-step solution strategy.

Case 5 is used to compare the solution results with the proposed strategy and those using the SNSA as a constraint.

In Fig. 15, the results of Cases 3, 4, and 5 are indicated by blue, yellow, and orange dots, respectively.

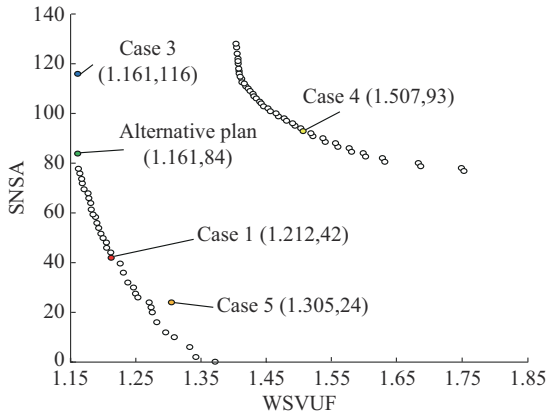

Fig. 15. Comparison of results of Cases 1, 3, 4, 5, and alternative plan.

In Case 3, compared with the final switching plan obtained in Case 1 (red dot in Fig. 15), the WSVUF is reduced by 4.21%, whereas the SNSA increases by 176.19%. From Fig. 15, we can observe that the blue dot has a certain distance from the Pareto front obtained in Case 1.

On the other hand, if the decision-maker is sensitive to the voltage unbalance issue and less concerned about the mechanical wear of the switches, an alternative plan can be selected, as shown in Fig. 15 (green dot), of which the WSVUF and SNSA are 1.161 and 84, respectively. The same values of WSVUF are obtained, but the proposed strategy outperforms the other in reducing SNSA by 27.59%.

In Case 4, it is difficult to obtain reliable results if the same population size and iteration limit as in Case 1 are used. If the iteration limit remains unchanged, even if the population size is increased to 1000, an obvious gap remains between the results in this case and those under the proposed solution strategy. Compared with the method without the two-step solution strategy, the proposed solution strategy reduces the WSVUF and SNSA by 19.58% and 54.84%, respectively. This comparison demonstrates the superiority of the proposed solution strategy.

In Case 5, a fixed SNSA threshold is set in a single solution, which is 42 in this case. In *Step 1*, the initial individual with $SNSA = 0$ is used to assist the algorithm in converging. Although a single switching plan can also be obtained with even more calculation time, a certain distance still remains between the dot and Pareto front obtained in Case 1. Furthermore, it is difficult to determine the value of the SNSA threshold. The constraint method uses only a certain threshold to limit the SNSA, which presents difficulties for the decision maker in knowing the effects of the change in the SNSA on the switching plan.

2) NLDC Method (Case 6)

Case 6 is used to compare the proposed strategy with the NLDC method [11]. In this case, the parameters are obtained by numerical fitting, and the voltage values of the voltage sources are regulated.

Because the NLDC method does not consider uncertainty, the power data of Scenario 1 are used to obtain the parameters, which are 0.7068, –0.6141, and 370.4030 after calculation. A comparison of the suppression effect on the WSVUF of the NLDC method and the proposed strategy is presented in Table II. Although the NLDC method inhibits the WSVUF (reduced by 45.98%), its effect is inferior to that of the strategy proposed in this paper (reduced by 87.34%). Global switching for the polarity of complex sources/loads is better than simply regulating the voltage source in terms of suppressing the WSVUF.

TABLE II
COMPARISON OF SUPPRESSION EFFECT ON WSVUF OF NLDC METHOD AND PROPOSED STRATEGY

Method/strategy	WSVUF
Without regulation	9.571
NLDC	5.170
Switching polarity (proposed strategy)	1.212

V. CONCLUSION

A day-ahead polarity switching strategy has been proposed in this paper to reduce voltage unbalance by optimally switching the polarity of the renewable generations and loads while minimizing the switching times simultaneously in the range of a full day. An effective two-step solution strategy is proposed for the multi-objective optimization problem. A new topology design of the SSD is shown to

achieve polarity switching and voltage stabilization. Case studies demonstrate the effectiveness of the proposed strategy. The key conclusions can be summarized as follows.

1) Compared with the method that ignores the SNSA, the proposed strategy can significantly reduce the mechanical wear of switches (SNSA is reduced by 63.79%) with a 4.39% compromise in the WSVUF. Thus, the service life can be extended.

2) Compared with the NLDC method, global switching for the polarity of complex sources/loads to reduce the WSVUF has a better global effect than simply regulating the voltage source.

3) The proposed two-step solution strategy effectively reduces the computational burden and improves the optimality of the results. Compared with the method without the two-step solution strategy, the WSVUF and SNSA are reduced by 19.58% and 54.84%, respectively. The time required to execute the calculation is reduced by 88.83%.

4) The SSD designed in this paper is effective in switching the polarity of the renewable generations and loads, maintaining operational stability during this process, and enabling unified switching.

APPENDIX A

TABLE AI
CONSTRAINT DATA IN CASE STUDIES

Constraint	Value
Voltage constraint of branches (+, –, *N*)	300 to 393.75 V (11-node), 637.5 to 787.5 V (34-node) –393.75 to –300 V (11-node), –787.5 to –637.5 V (34-node) –75 to 18.75 V (11-node), –112.5 to 37.5 V (34-node)
Voltage constraint of sources/loads (*p*, *n*, *b*)	300 to 393.75 V (11-node), 637.5 to 787.5 V (34-node) 300 to 393.75 V (11-node), 637.5 to 787.5 V (34-node) 600 to 787.5 V (11-node), 1275 to 1575 V (34-node)
Branch current constraint	230 A
VUF constraint of every node	3%

TABLE AII
PARAMETER SETTINGS AND TIME REQUIRED WITH GA

Case	Step	Parameter	Value	Time (s)
1	*Step 1*	Population size	150 for the first time interval in the previous calculation of the first part; 100 for other time intervals in the previous calculation of the first part; 300 for the first part; 50 for the second part	1793
		Iteration limit	50 for the previous calculation of the first part; 100 for the first part; 50 for the second part	
	Step 2	Population size	100	
		Iteration limit	150	
2	*Step 1*	Population size	450 for the first time interval in the previous calculation of the first part; 400 for other time intervals in the previous calculation of the first part; 400 for the first part; 400 for the second part	26673
		Iteration limit	150 for the previous calculation of the first part; 100 for the first part; 100 for the second part	
	Step 2	Population size	100	
		Iteration limit	150	
3		Population size	100	540
		Iteration limit	50	
4		Population size	1000	16050
		Iteration limit	150	
5	*Step 1*	Population size	50	2067
		Iteration limit	50	
	Step 2	Population size	300	
		Iteration limit	100	

REFERENCES

[1] L. Zhang, J. Liang, W. Tang *et al*., "Converting AC distribution lines to DC to increase transfer capacities and DG penetration," *IEEE Transactions on Smart Grid*, vol. 10, no. 2, pp. 1477-1487, Mar. 2019.

[2] J. Liao, N. Zhou, Q. Wang *et al*., "Load-switching strategy for voltage balancing of bipolar DC distribution networks based on optimal automatic commutation algorithm," *IEEE Transactions on Smart Grid*, vol. 12, no. 4, pp. 2966-2979, Jul. 2021.

[3] E. Rodriguez-Diaz, M. Savaghebi, J. C. Vasquez *et al*., "An overview of low voltage DC distribution systems for residential applications," in *Proceedings of 2015 IEEE 5th International Conference on Consumer Electronics*, Berlin, Germany, Sept. 2015, pp. 318-322.

[4] S. Rivera, R. Lizana F., S. Kouro *et al*., "Bipolar DC power conversion: state-of-the-art and emerging technologies," *IEEE Journal of Emerging and Selected Topics in Power Electronics*, vol. 9, no. 2, pp. 1192-1204, Apr. 2021.

[5] J. Liao, N. Zhou, Y. Huang *et al*., "Unbalanced voltage suppression in a bipolar DC distribution network based on DC electric springs," *IEEE Transactions on Smart Grid*, vol. 11, no. 2, pp. 1667-1678, Mar. 2020.

[6] J.-Y. Lee, Y.-P. Cho, and J.-H. Jung, "Single-stage voltage balancer with high-frequency isolation for bipolar LVDC distribution system," *IEEE Transactions on Industrial Electronics*, vol. 67, no. 5, pp. 3596-3606, May 2020.

[7] Z. Pei, X. Song, C. Liu *et al*., "Self-balancing isolated DC-DC con-

verter for bipolar low voltage DC microgrid," *Electric Power Automation Equipment*, vol. 42, no. 5, pp. 47-53, Feb. 2022.
[8] J. Liao, Z. Qin, P. Purgat *et al*., "Unbalanced voltage/power control in bipolar DC distribution grids using power flow controller," in *Proceedings of 2020 IEEE 29th International Symposium on Industrial Electronics (ISIE)*, Delft, Netherlands, Jun. 2020, pp. 1290-1295.
[9] X. Zhang, C. Gong, and Z. Yao, "Three-level DC converter for balancing DC 800-V voltage," *IEEE Transactions on Power Electronics*, vol. 30, no. 7, pp. 3499-3507, Jul. 2015.
[10] P. Prabhakaran and V. Agarwal, "Mitigation of voltage unbalance in a low voltage bipolar DC microgrid using a boost-SEPIC type interleaved DC-DC compensator," in *Proceedings of 2016 IEEE 2nd Annual Southern Power Electronics Conference (SPEC)*, Auckland, New Zealand, Dec. 2016, pp. 1-6.
[11] T.-H. Jung, G.-H. Gwon, C.-H. Kim *et al*., "Voltage regulation method for voltage drop compensation and unbalance reduction in bipolar low-voltage DC distribution system," *IEEE Transactions on Power Delivery*, vol. 33, no. 1, pp. 141-149, Feb. 2018.
[12] G.-H. Gwon, C.-H. Kim, Y.-S. Oh *et al*., "Mitigation of voltage unbalance by using static load transfer switch in bipolar low voltage DC distribution system," *International Journal of Electrical Power & Energy Systems*, vol. 90, pp. 158-167, Sept. 2017.
[13] B. S. H. Chew, Y. Xu, and Q. Wu, "Voltage balancing for bipolar DC distribution grids: a power flow based binary integer multi-objective optimization approach," *IEEE Transactions on Power Systems*, vol. 34, no. 1, pp. 28-39, Jan. 2019.
[14] Z. Zhang, D. Mei, H. Jiang *et al.*, "Mode for reducing wind curtailment based on battery transportation," *Journal of Modern Power Systems and Clean Energy*, vol. 6, no. 6, pp. 1158-1171, Nov. 2018.
[15] T. Zhu, Z. Yu, R. Zeng *et al*., "Transient model and operation characteristics researches of hybrid DC circuit breaker," *Proceedings of the CSEE*, vol. 36, no. 1, pp. 18-30, Jan. 2016.
[16] H. Haghnazari, R. Lazzari, and L. Piegari, "Design of LVDC bidirectional hybrid circuit breaker," in *Proceedings of 2021 IEEE Fourth International Conference on DC Microgrids (ICDCM)*, Arlington, USA, Jul. 2021, pp. 1-7.
[17] R. Lazzari and L. Piegari, "Design and implementation of LVDC hybrid circuit breaker," *IEEE Transactions on Power Electronics*, vol. 34, no. 8, pp. 7369-7380, Aug. 2019.
[18] C. F. Ionescu, C. Bulac, F. Capitanescu *et al*., "Multi-period power loss optimization with limited number of switching actions for enhanced continuous power supply," in *Proceedings of 2014 16th International Conference on Harmonics and Quality of Power (ICHQP)*, Bucharest, Romania, May 2014, pp. 34-38.
[19] A. Vanin, "Volt/var control method considering limited switching operations based on the cluster approach," in *Proceedings of 2017 International Siberian Conference on Control and Communications (SIBCON)*, Astana, Kazakhstan, Jun. 2017, pp. 1-4.
[20] L. Liu, C. Peng, Z. Wen *et al*., "Distributed photovoltaic consumption strategy based on dynamic reconfiguration of distribution network," *Electric Power Automation Equipment*, vol. 39, no. 12, pp. 56-62, Dec. 2019.
[21] S. Pang, W. Li, H. He *et al*., "An EDA-GA hybrid algorithm for multi-objective task scheduling in cloud computing," *IEEE Access*, vol. 7, pp. 146379-146389, Oct. 2019.
[22] J.-O. Lee, Y.-S. Kim, and S.-I. Moon, "Current injection power flow analysis and optimal generation dispatch for bipolar DC microgrids," *IEEE Transactions on Smart Grid*, vol. 12, no. 3, pp. 1918-1928, May 2021.
[23] X. Ai, B. Tayierjiang, L. Yang *et al*., "Optimizing the spinning reserve in wind power system using scenario method," *Power System Technology*, vol. 42, no. 3, pp. 835-841, Mar. 2018.
[24] X. Chen, Q. Xu, and Y. Yang, "Day-ahead optimized economic dispatch of CCHP microgrid considering wind power uncertainty," *Electric Power Construction*, vol. 41, no. 6, pp. 107-113, Jun. 2020.
[25] Y. Li, Y. Cai, T. Zhao *et al.*, "Multi-objective optimal operation of centralized battery swap charging system with photovoltaic," *Journal of Modern Power Systems and Clean Energy*, vol. 10, no. 1, pp. 149-162, Jan. 2022.
[26] A. M. Dissanayake and N. C. Ekneligoda, "Multiobjective optimization of droop-controlled distributed generators in DC microgrids," *IEEE Transactions on Industrial Informatics*, vol. 16, no. 4, pp. 2423-2435, Apr. 2020.
[27] R. Wang and Y. Liu. "Analysis and comparison of DC interruption techniques of switches," *Electrical Engineering Materials*, vol. 2011, no. 4, pp. 40-45, Dec. 2011.
[28] M. Rong, F. Yang, Y. Wu *et al*., "Switching arc phenomenon in DC circuit breaker," in *Proceedings of the XIX International Conference on Gas Discharges and Their Applications*, Beijing, China, Sept. 2012, pp. 29-36.
[29] J. Liao, N. Zhou, Q. Wang *et al*., "Definition and correlation analysis of power quality index of DC distribution network," *Proceedings of the CSEE*, vol. 38, no. 23, pp. 6847-6860, Dec. 2018.

Zhongchi Huang received the B.E. degree in electrical engineering and automation from Chongqing University, Chongqing, China, in 2020. He is currently purchasing the Master's degree of engineering from Chongqing University. His research interests include analysis and operation of power systems, and power quality of DC distribution network.

Qianggang Wang received the B. S. and Ph. D. degrees from Chongqing University, Chongqing, China, in 2009 and 2015, respectively. He is currently working as an Associate Professor in Chongqing University. His research interests include analysis and operation of power systems, microgrids, and power quality.

Yuan Chi received the B.E. degree from Southeast University, Nanjing, China, in 2009, the M.E. degree from Chongqing University, Chongqing, China, in 2012, and the Ph.D. degree from Nanyang Technological University, Singapore, in 2021. He is currently working as a Research Associate with Chongqing University. His research interests include planning and resilience of power system, and voltage stability.

Jianquan Liao received the B.S. degree in electrical engineering from the China University of Petroleum, Qingdao, China, in 2017, and the Ph.D. degree from Chongqing University, Chongqing, China, in 2021. He is currently working as an Associate Research Fellow in Sichuan University, Chengdu, China. His research interests include power system protection and control, power quality of DC distribution network, and power system stability and control.

Yu Zhang received the B.E. degree in electrical engineering and automation from Chongqing University, Chongqing, China, in 2019, and the Master's degree of engineering from Chongqing University in 2022. He is currently working as an Electrical Engineer at State Grid Chongqing Shibei Electric Power Supply Branch, Chongqing, China. His research interests include analysis and operation of power systems, DC microgrids, and power quality.

Niancheng Zhou received the B.S., M.S., and Ph.D. degrees from Chongqing University, Chongqing, China, in 1991, 1994, and 1997, respectively. He is currently working as a Professor in Chongqing University. His research interests include analysis and operation of power systems, microgrids, and power quality.